

Article

Study on Annular Pressure Buildup in Offshore Heavy Oil Thermal Recovery Wells Considering Dissolved Gas Contained in Annuli

Hao Wang ^{1,2} , Hui Zhang ^{1,*}, Jun Li ¹, Anming Chen ³, Jun Liu ³, Tengfei Sun ⁴ and Cong Lin ⁵

¹ College of Petroleum Engineering, China University of Petroleum-Beijing, Beijing 102249, China; 2017312032@student.cup.edu.cn (H.W.); lijuncup2018@163.com (J.L.)

² MOE Key Laboratory of Petroleum Engineering, China University of Petroleum-Beijing, Beijing 102249, China

³ Sinopec Huadong Oilfield Service Corporation, Nanjing 210000, China; chenam.oshd@sinopec.com (A.C); liu8xu8jun@126.com (J.L.)

⁴ College of Mechanical and Electrical Engineering, Beijing University of Chemical Technology, Beijing 100029, China; suntengfei@mail.buct.edu.cn

⁵ AVIC China Aero-Polytechnology Establishment, Beijing 100028, China; Linc@cape.avic.com

* Correspondence: zhanghuicup2018@163.com; Tel.: +86-132-6932-0820

Abstract: In the offshore industry, especially heavy oil thermal recovery wells, due to the great temperature difference between the low-temperature seawater and high-temperature heavy oil, it is easy to cause the temperature increase of annular fluid in the operation process which will result in the annular pressure buildup phenomenon (APB). The increase of annulus pressure may lead to the failure of the casing and wellbore integrity, which will seriously affect the normal production and lead to great economic loss. In order to study the formation of APB and provide a basis for the field operation design, a radial full-size physical experiment of APB was carried out in this work and an annular pressure prediction model in the presence of dissolved gas was proposed based on the experimental results. The verification and comparison analyses of the full-liquid model and the dissolved gas model were conducted with the experimental data. Furthermore, the sensitivity analysis of the influence of the dissolved gas volume fraction and casing deformation on APB was carried out. The results show that the prediction results calculated by the dissolved gas model are in good agreement with the experimental data and the prediction accuracy is higher than that of the full-liquid model. When the annular dissolved gas volume fraction is less than 0.1%, the full-liquid model can be used to simplify and approximate calculations. Ignoring casing deformation will produce prediction error in each annulus, which means this simplification should be used with extreme caution. This work provides a valuable experimental reference for the study of APB, as well as a novel model for APB prediction in the field.

Keywords: annular pressure buildup; dissolved gas; experiment verification; offshore wells; casing deformation



Citation: Wang, H.; Zhang, H.; Li, J.; Chen, A.; Liu, J.; Sun, T.; Lin, C. Study on Annular Pressure Buildup in Offshore Heavy Oil Thermal Recovery Wells Considering Dissolved Gas Contained in Annuli. *Energies* **2021**, *14*, 3213. <https://doi.org/10.3390/en14113213>

Academic Editor: Reza Rezaee

Received: 26 April 2021

Accepted: 27 May 2021

Published: 31 May 2021

Publisher's Note: MDPI stays neutral with regard to jurisdictional claims in published maps and institutional affiliations.



Copyright: © 2021 by the authors. Licensee MDPI, Basel, Switzerland. This article is an open access article distributed under the terms and conditions of the Creative Commons Attribution (CC BY) license (<https://creativecommons.org/licenses/by/4.0/>).

1. Introduction

With the development of offshore oil and gas, the exploration is moving into the deep sea [1–3]. In the development, the temperature and pressure are important factors that influence the drilling and production operations [4,5]. In recent years, the problem of annular pressure buildup (APB) has attracted more and more attention [6–10], especially in thermal recovery wells. APB refers to the phenomenon of pressure increase caused by the expansion of trapped fluid existing in the casing annuli [11,12]. Casing annuli are created as a result of the cementing and completion operation [13–16]. A typical wellbore structure of subsea wells is shown in Figure 1. The fluid thermal expansion is mainly caused by temperature increase due to the field operations such as steam injection [17,18].

APB is a serious threat to wellbore integrity [19,20]. It may lead to a rapid increase of casing pressure and cause casing collapse and failure [21,22], which may seriously affect the regular production operations and even lead to well abandonment. It is a great safety risk, and any kind of accident caused by APB usually leads to significant economic losses [23,24]. While drilling on Pompano A-31 in the Gulf of Mexico, the 16-in casing was collapsed because of the APB [9]. Similarly, a casing failure caused by APB also occurred in the Marlin A-2 well [25,26]. In offshore environments, costs and safety requirements of oil and gas development are even higher. Meanwhile, the temperature change of annular fluid is larger than in most land wells because of the lower temperature of the seawater [27,28]. The pressure release operation is also complicated, especially for annuli B and C [6,28]. Therefore, APB has to be settled urgently and the study on this problem is of great engineering and economic significance.

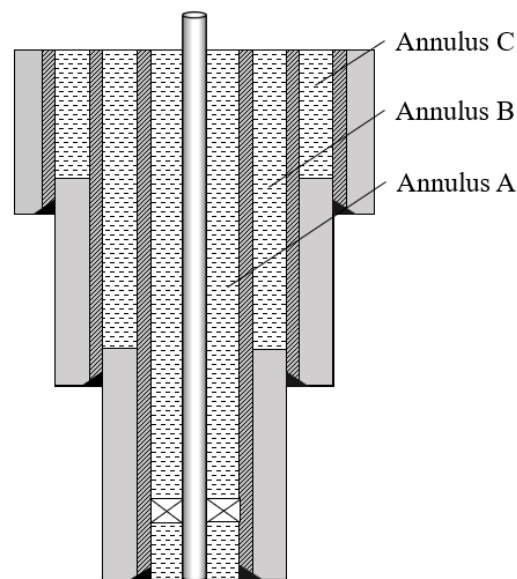


Figure 1. Typical wellbore structure of subsea wells.

In recent years, many scholars have analyzed the formation mechanism of APB and established different prediction models. Oudemans et al. analyzed the main causes of APB and proposed a model to analyze and predict APB in annuli [7]. Wang et al. analyzed the optimal nitrogen volume when adopting the nitrogen injection method to control APB and proposed a calculation method to predict APB in gas liquid two-phase annulus [27]. Kan et al. studied the effect of different production parameters on APB based on numerical simulation and conducted experiments to analyze a novel method for controlling APB [29]. Yin et al. considered the change of the water thermal expansibility and compressibility with the temperature and then improved the calculation precision of APB [30]. Liu et al. analyzed influence of the production rate, well depth, and annulus length on APB [31]. Zhang et al. established a calculation model to predict the wellbore temperature and further studied APB and its influence factors with a case study [32]. Gao et al. proposed a model to calculate APB and studied the strength and safety of the casing under the pressure caused by APB [33]. Wang et al. considered the change of the annular fluid compressibility and expansibility and improved the prediction model. Then, APB in annuli full of liquid or containing gas were analyzed based on physical experiments [34,35].

At present, there are few experimental studies related to the APB and most of them only focus on a single annulus, which leads to the lack of experimental verification for the coupling effect of casing deformation. Wang et al. used a cylindrical pressure vessel filled with water to conduct experiments [34,35]. Vargo et al. conducted experiments with an autoclave setup to study pressure buildup of different fluids containing different volume of nitrogen [36]. Their papers both provided valuable data for APB analysis, but the setups

used were simple and their simulations of the wellbore structure are not good. Most of the research on APB is theoretical and it can be divided into two categories. One is for the case where the annulus is full of liquid. The model used in this case is an equation derived from the equation of state (EOS). The isobaric thermal expansion coefficient and isothermal compression coefficient are often treated as constant in most papers; however, there is a lack of the consideration of the variability of the fluid compressibility and expansibility. The other case considers two phases (gas and liquid) existing in the annulus. In the latter, pressure buildup of the annular gas is calculated by using the EOS, and the key point is to determine the compression factor. Meanwhile, the gas in annuli is assumed to be injected by operation and the gas dissolved in liquid is ignored because of its tiny volume in most of the studies. Something that also happened in some papers related to the full-liquid case was that annuli were treated as a trapped space with no gas existing. However, it is still found that there is not always no gas in each annulus in this work. In most cases, trace amounts of gas exist [35], and they are believed to be dissolved gas in the water in this work. The presence of dissolved gas has a direct impact on the early annulus pressure increase and significantly influences the final prediction results, which should not be ignored in the field.

In this paper, a radial full-size tri-annulus APB experiment was carried out to study APB phenomenon firstly. Then, the change of expansibility and compressibility of annular fluid with temperature and pressure was considered by using a similar method as that adopted in some research [34,35,37]; the isothermal compression coefficient and isobaric thermal expansion coefficient were fitted by the data found in the related research [34,35]. The full-liquid prediction equation was modified according to theoretical derivation, and a prediction model of APB considering the existence of dissolved gas was proposed further. These two pressure prediction models under different conditions were both studied through the experimental data analysis and were verified to have high prediction accuracy. Finally, the sensitivity analysis was conducted to study the influence of dissolved gas volume fraction and casing deformation on APB. The results show that dissolved gas does exist in this experiment and has an important influence on the prediction of APB, which should be considered in the field operation design. The research in this paper can provide some reference and experimental basis for field operations.

2. Experiments

2.1. Experiment Preparation

A new setup was developed to carry out experiments on the annular pressure buildup and casing-cement cementing load. The setup and its structure are shown in Figure 2. The setup schematic and the positions of annuli A, B, and C are shown in Figure 3.

A typical tri-annulus structure in the field well can be simulated through this setup. The setup has independent temperature and pressure sensors for each annulus to measure values in real time during the experiment. The resolution of the temperature and pressure measurements are 1 °C and 0.001 MPa, respectively. In the experiment, P110 tubing and casings were used to simulate the wellbore structure (the casing actually adopted is shown in Figure 4), and their dimensions and material properties are shown in Table 1. A multiple sealing design was adopted at both ends of the casing in order to ensure the effective sealing of annuli. As a result, the fluid could be trapped in each annulus under high temperature and pressure for a long time.

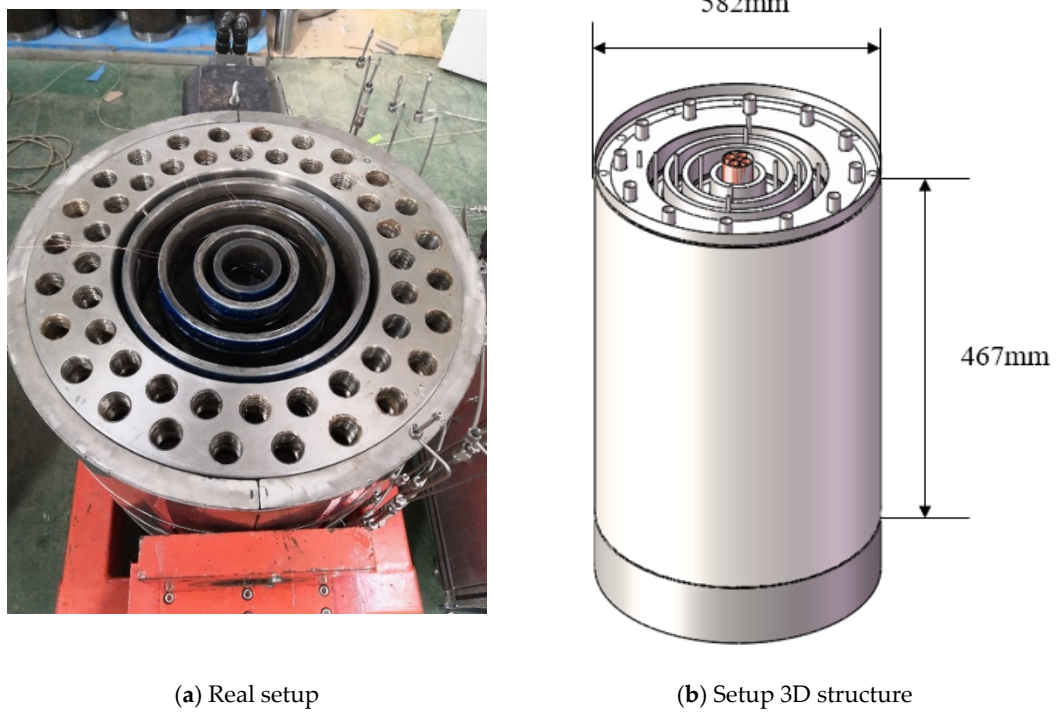


Figure 2. APB and casing-cement cementing load test setup.

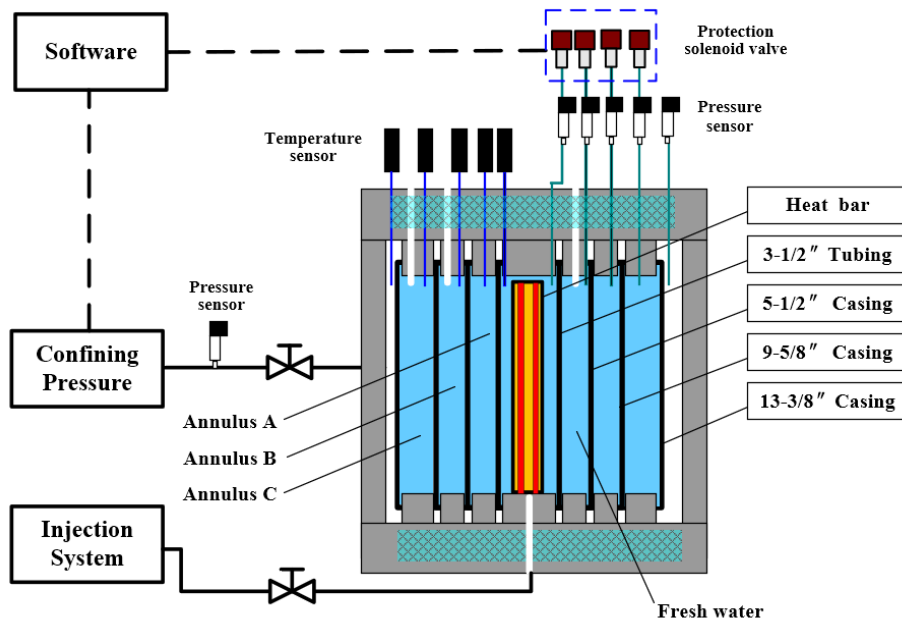


Figure 3. The schematic of the experimental setup.



Figure 4. The casing actually adopted in the experiment.

Table 1. Material properties of adopted casing.

Grade	Length (mm)	The Outer Diameter (mm)	Thickness (mm)	Modulus of Elasticity (MPa)	Poisson's Ratio	Coefficient of Thermal Expansion
P110	467	88.9	6.50	210,000	0.3	0.000012
P110	467	139.7	6.20	210,000	0.3	0.000012
P110	467	244.5	13.85	210,000	0.3	0.000012
P110	467	339.7	12.20	210,000	0.3	0.000012

2.2. Experimental Procedure

Since most of the field annuli are trapped and filled with liquid after cementing [38–40], and the thermal properties of synthetic drilling fluid are similar to those of water according to the related research [30,41], fresh water (1.01 g/cm^3) at room temperature ($37.0 \text{ }^\circ\text{C}$) was used to fill A, B, and C annuli to simulate field conditions. Meanwhile, there was no confining pressure in the experiment. Note that the water was filled with a circulating method (injected from the bottom and flowed out from the top) while the setup was placed horizontally. Therefore, one can consider that the influence of residual gas was eliminated. Considering that the temperature changes radially from the center of the wellbore to the outside in actual field operations, the setup was preheated in the experiment in order to simulate the actual annulus temperature distribution. The fluid temperature in the tubing was set at $100 \text{ }^\circ\text{C}$ initially and gradually increased to $160.0 \text{ }^\circ\text{C}$ during the experiment and data were recorded periodically.

Since four layers of P110 tubing and casings were used and three annuli were constructed in the experiment, pressure in each annulus affects the others due to the deformation of the casing. This experiment can be used not only to explore the multiple APB phenomena, but also to investigate the influence of casing deformation on APB. Figure 5 shows the picture of the setup when installation was completed, and annuli were sealed.



Figure 5. The sealed setup filled with water in three annuli.

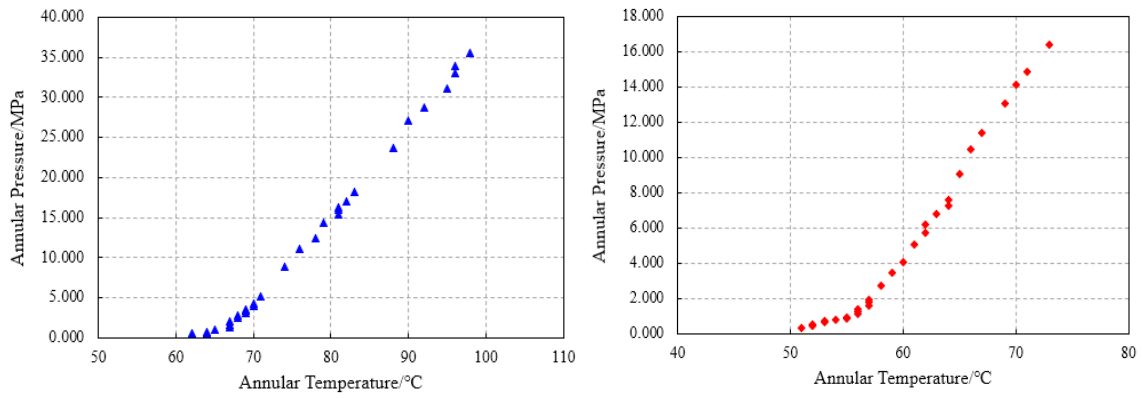
3. Experimental Results and Discussion

3.1. Experimental Results

During the experiment, the pressures in A, B, and C annuli were measured in real time. Temperature and pressure data for each annulus are shown in Table 2. The pressure–temperature scatter plots are shown in Figure 6. The change of annular temperature with the time is shown in Figure 7.

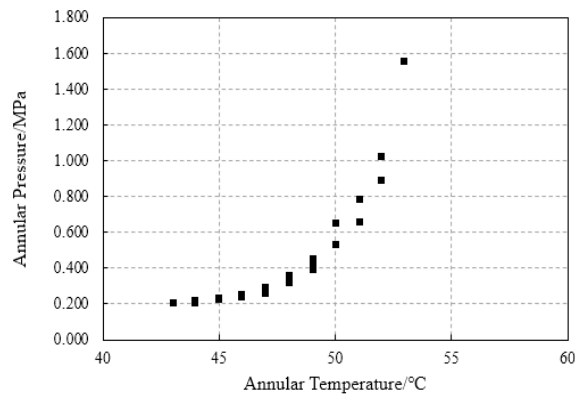
The experimental results show that pressure is positively correlated with temperature increase. It is obvious that the A annular pressure increases the fastest (up to 35.466 MPa) and the C annular pressure increases the least (up to 1.556 MPa), while the temperature of the fluid in the tubing increases from 100 °C to 160 °C. It is influenced by the heat transfer characteristics of the experimental setup. The heat transfers from the center to the outside in the experiment, leading to the maximum temperature in annulus A (up to 98 °C) and the minimum temperature in annulus C (up to 53 °C).

With the increase of temperature, the pressure increase rate gradually accelerates and finally tends to be stable, which makes the pressure–temperature scatter plots approximately linear after a small initial bend. The existence of this bend directly affects the final pressure value under a certain temperature increment. Similar phenomena have occurred in some studies [7,35]. Further study on this phenomenon was conducted in this work.



(a) The experimental data of annulus A

(b) The experimental data of annulus B



(c) The experimental data of annulus C

Figure 6. The experimental pressure–temperature scatter plots for each annulus.

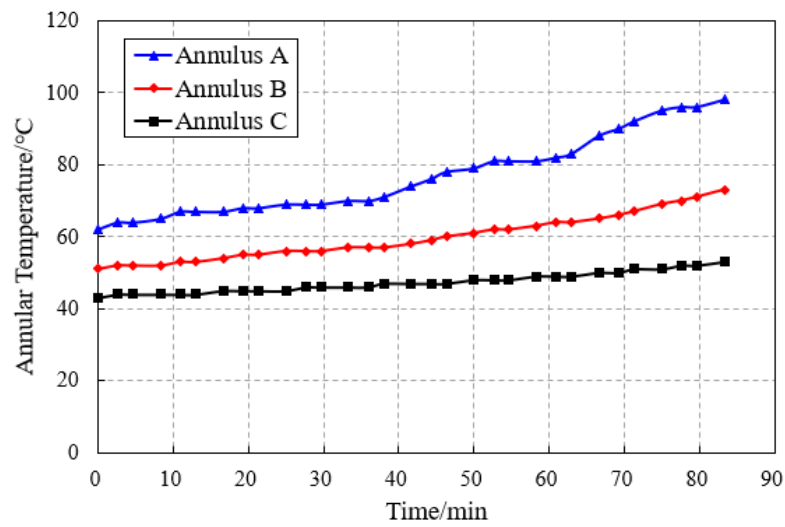


Figure 7. The change of annular temperature with the time.

Table 2. Experimental data of temperature and pressure of each annulus.

T-Tubing Fluid (°C)	P-Tubing Fluid (MPa)	T-A Annulus (°C)	P-A Annulus (MPa)	T-B Annulus (°C)	P-B Annulus (MPa)	T-C Annulus (°C)	P-C Annulus (MPa)
160	29.919	98	35.466	73	16.410	53	1.556
158	30.134	96	33.881	71	14.846	52	1.021
158	30.279	96	33.029	70	14.113	52	0.888
156	25.072	95	31.157	69	13.036	51	0.784
152	25.166	92	28.707	67	11.407	51	0.655
151	25.375	90	27.029	66	10.447	50	0.649
148	20.973	88	23.629	65	9.078	50	0.531
136	21.064	83	18.207	64	7.617	49	0.448
130	17.095	82	17.034	64	7.248	49	0.421
130	16.149	81	16.297	63	6.819	49	0.390
131	15.970	81	16.041	62	6.199	48	0.353
131	15.167	81	15.339	62	5.741	48	0.335
129	14.177	79	14.322	61	5.077	48	0.314
129	12.228	78	12.462	60	4.066	47	0.289
125	10.851	76	11.158	59	3.475	47	0.279
123	8.244	74	8.918	58	2.711	47	0.266
114	6.423	71	5.204	57	1.942	47	0.256
110	3.959	70	4.286	57	1.777	46	0.251
110	3.910	70	4.029	57	1.614	46	0.246
110	2.908	69	3.602	56	1.385	46	0.240
109	2.900	69	3.388	56	1.266	46	0.237
109	2.928	69	3.108	56	1.115	45	0.232
108	3.085	68	2.715	55	0.922	45	0.226
107	1.909	68	2.419	55	0.831	45	0.223
107	1.983	67	2.114	54	0.768	45	0.220
106	0.954	67	1.620	53	0.710	44	0.215
106	0.975	67	1.375	53	0.651	44	0.212
105	0.622	65	1.021	52	0.550	44	0.208
104	0.546	64	0.689	52	0.436	44	0.204
102	0.451	64	0.609	52	0.430	44	0.203
100	0.310	62	0.507	51	0.338	43	0.201

T-A annulus refers to the temperature of fluid in annulus A; P-A annulus refers to the pressure of fluid in annulus A.

3.2. Full-Liquid Model Analysis

So far, most scholars have used Equation (1) to calculate the APB in annuli [8,29,32]. This equation is obtained according to the EOS [7]. It is often used when isobaric thermal expansion coefficient and isothermal compression coefficient of water are constant. Some scholars further treat those two coefficients as functions of the temperature and pressure [34,35,37]. The calculation error is reduced but still not eliminated.

$$\Delta P = \frac{\alpha_{isob}}{k_{isot}} \Delta T - \frac{1}{k_{isot} V_{ann}} \Delta V_{ann} + \frac{1}{k_{isot} V_l} \Delta V_l \quad (1)$$

In this work, a modified integral model based on the EOS was used to analyze the experimental data of APB. As each annulus was sealed, the mass of fluid was considered constant. According to the EOS, the pressure is a function of temperature and fluid volume.

$$P = f(T, V) \quad (2)$$

The APB process can be regarded as the combination of two steps, which are isobaric expansion and isothermal compression. The process is shown schematically in Figure 8.

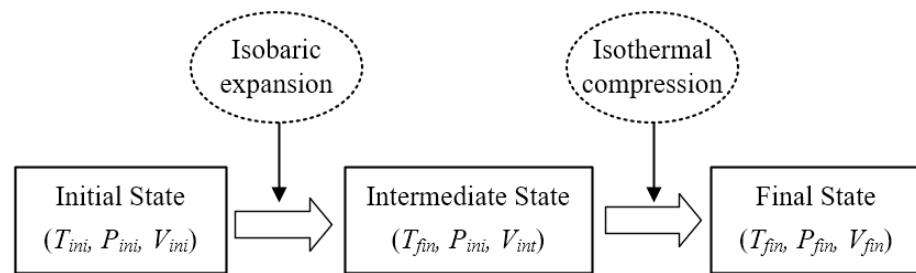


Figure 8. APB stepwise process diagram.

Equation (2) can be rewritten as follows, using partial differential and integral operations.

$$\int_{t_{ini}}^{t_{fin}} \alpha_{isob} dt - \int_{P_{ini}}^{P_{fin}} k_{isot} dP = \ln \left(\frac{V_{fin}}{V_{ini}} \right) \quad (3)$$

In Equation (3), the isobaric thermal expansion coefficient and isothermal compression coefficient are regarded as functions of temperature and pressure. Equations (5) and (6) are fitted formulas obtained according to the data from related researches [34,35], which will be more suitable for iterative computation.

$$t = T - 273.15 \quad (4)$$

$$\alpha_{isob}(P, t) = a_1 + b_1 t + c_1 P + d_1 t^2 + e_1 t P + f_1 t^3 + g_1 t^2 P \quad (5)$$

$$k_{isot}(P, t) = a_2 + b_2 t + c_2 P + d_2 t^2 + e_2 t P + f_2 t^3 + g_2 t^2 P \quad (6)$$

The fitting coefficients in those formulas are shown in Table 3.

Table 3. Fitting coefficients.

	α_{isob}	k_{isot}
<i>a</i>	-1.337×10^{-5}	4.943×10^{-4}
<i>b</i>	1.200×10^{-5}	-2.335×10^{-6}
<i>c</i>	1.908×10^{-6}	-1.187×10^{-6}
<i>d</i>	-6.343×10^{-8}	2.548×10^{-8}
<i>e</i>	-3.883×10^{-8}	7.989×10^{-9}
<i>f</i>	2.036×10^{-10}	-2.670×10^{-11}
<i>g</i>	6.804×10^{-11}	-1.083×10^{-10}
Fitting R^2	0.9995	0.9757

The coefficient of α_{isob} is subscripted as 1 and the coefficient of k_{isot} is subscripted as 2 in Equations (5) and (6).

As is shown in Figure 8, the pressure in the isobaric expansion process is taken as P_{ini} , and the temperature in the isothermal compression process is taken as T_{fin} . The first two terms in Equation (3) can be obtained as follows:

$$t = T - 273.15 \quad (7)$$

$$\int_{t_{ini}}^{t_{fin}} \alpha_{isob} dt = (a_1 + c_1 P_{ini})t + \left(\frac{b_1}{2} + \frac{e_1 P_{ini}}{2} \right) t^2 + \left(\frac{d_1}{3} + \frac{g_1 P_{ini}}{3} \right) t^3 + \frac{f_1}{4} t^4 \quad (8)$$

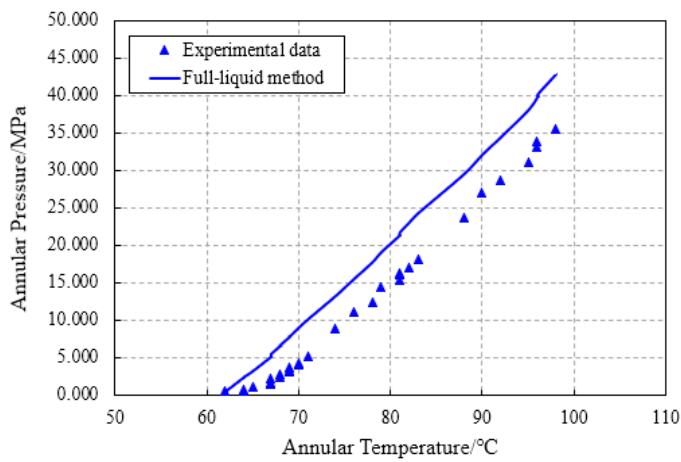
$$\int_{P_{ini}}^{P_{fin}} k_{isot} dP = \left(a_2 + b_2 t_{fin} + d_2 t_{fin}^2 + f_2 t_{fin}^3 \right) P + \left(\frac{c_2}{2} + \frac{e_2 t_{fin}}{2} + \frac{g_2 t_{fin}^2}{2} \right) P^2 \quad (9)$$

The final volume of fluid could be obtained by casing deformation calculations. The casing deformation is caused by internal and external pressure and thermal expansion. The calculation formulas are as follows [42]:

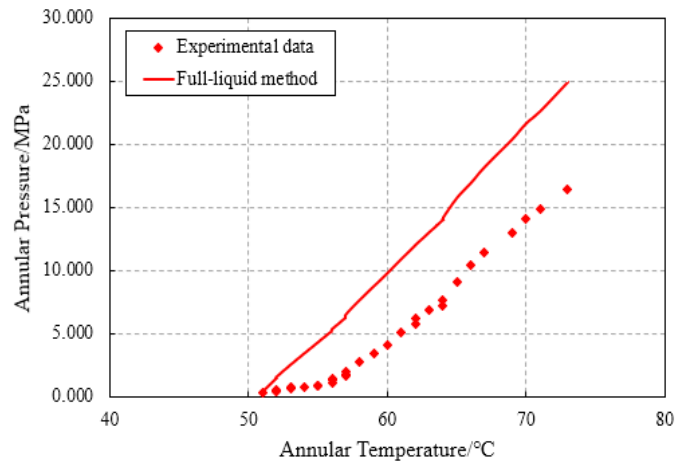
$$u_t = \frac{1 + \mu}{1 - \mu} \frac{\alpha_c}{r} \int_{r_i}^r \Delta T r dr \tag{10}$$

$$u_p = \frac{1}{E} \left[-(1 + \mu) \frac{r_i^2 r_o^2 (P_o - P_i)}{r_o^2 - r_i^2} \frac{1}{r} + (1 - \mu) \frac{r_i^2 P_i - r_o^2 P_o}{r_o^2 - r_i^2} r \right] \tag{11}$$

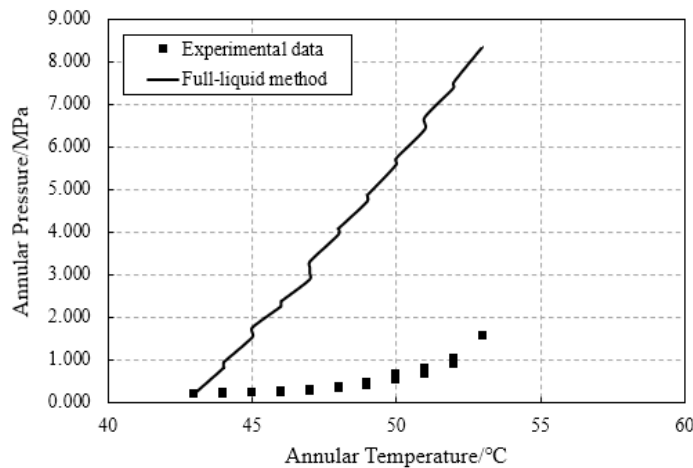
This model was used to perform the calculation and analysis. The results are shown in Figure 9.



(a) The calculated results of annulus A;



(b) The calculated results of annulus B



(c) The calculated results of annulus C

Figure 9. Comparison of the full-liquid model simulations with experimental data.

The error analysis of the calculated results is shown in Table 4.

Table 4. The error analysis of simulations using the full-liquid model.

Annulus	RMSE (MPa)	Final Prediction Error (MPa)
A	5.043	7.433
B	5.291	8.524
C	3.683	6.786

RMSE: root mean square error.

As is shown in Figure 9 and Table 4, calculations using the full-liquid model overestimate the experimental data in each annulus. The RMSE of annulus A is similar to that of annulus B, but it is important to note that the maximum pressure in annulus B is 16.410 MPa, less than that of annulus A, which means the relative error of annulus B is larger. Similarly, the maximum experimental pressure in annulus C is 1.556 MPa and the final prediction error reaches 6.786 MPa, which also leads to a significant relative error.

It is concluded that using the full-liquid model to predict the APB can lead to a very conservative assessment, leading to the adoption of inappropriate prevention measures and even the giving up of feasible solutions. It may result in the loss of economic and human resources. Considering the actual situation in the field, the pressure adjustment operations are easier to conduct in annulus A compared to annuli B and C, which means the APB in annulus B and C is more difficult to release.

3.3. Dissolved Gas Model Analysis

According to the above theoretical approach, the prediction of APB using the full-liquid model is not very accurate, leading to significant prediction errors in different annuli. On the experimental curves, one can notice there is a small bend at the initial stage of pressure increase. It is one of the important factors leading to the prediction error. To address this discrepancy, the dissolved gas in fresh water was considered and analyzed in this study. Dissolved gas is invisible when dissolved in water, and thus difficult to observe directly, which makes it is easy to ignore its effect on APB.

The main component of the air is nitrogen, and its proportion reaches around 78%. Therefore, dissolved gas was treated as nitrogen in this study. The solubility of nitrogen in fresh water at 0.1 MPa can be obtained from Equation (12) [43]:

$$\ln C = A_0 + A_1 T_s + A_2 T_s^2 + A_3 T_s^3 \quad (12)$$

where T_s is a formula parameter, as follows:

$$T_s = \ln \left(\frac{298.15 - t}{273.15 + t} \right) \quad (13)$$

The gas properties are calculated by the PR EOS [44], which is

$$P = \frac{RT}{\tilde{v} - b} - \frac{a_c a}{\tilde{v}^2 + 2b\tilde{v} - b^2} \quad (14)$$

The compression factor can be obtained as follows.

$$Z^3 - (1 - B)Z^2 + (A - 2B - 3B^2)Z - (AB - B^2 - B^3) = 0 \quad (15)$$

where

$$\tilde{v} = \frac{ZRT}{P} \quad (16)$$

$$A = \frac{0.457235aP_r}{T_r^2}, B = \frac{0.077796P_r}{T_r} \quad (17)$$

Annuli were filled with fresh water at room temperature (37 °C) and adjusted to the initial temperature and pressure. The molar volume of the dissolved gas, both at room

temperature and under initial condition, can be obtained using Equations (15) and (16). Then, the dissolved gas volume fraction at room temperature and under initial condition can be obtained by Equations (12) and (14). Results are shown in Table 5.

Table 5. The initial condition of fluid in each annulus.

Annulus	Initial Temperature (°C)	Initial Pressure (MPa)	Dissolved Gas Volume Fraction under Initial Condition
A	62	0.507	0.228%
B	51	0.338	0.331%
C	43	0.201	0.543%

The initial temperature of the water is 37 °C.

The final pressure in the annulus was set as P and the change in the molar volume of dissolved gas was calculated, which is caused by the casing deformation and the change in liquid volume. The casing deformation can be obtained from Equations (10) and (11), while the change in liquid volume can be obtained from Equation (3). Eventually, the final annular pressure P' can be calculated by iterating three coupled annulus pressures. The calculation process is shown in Figure 10.

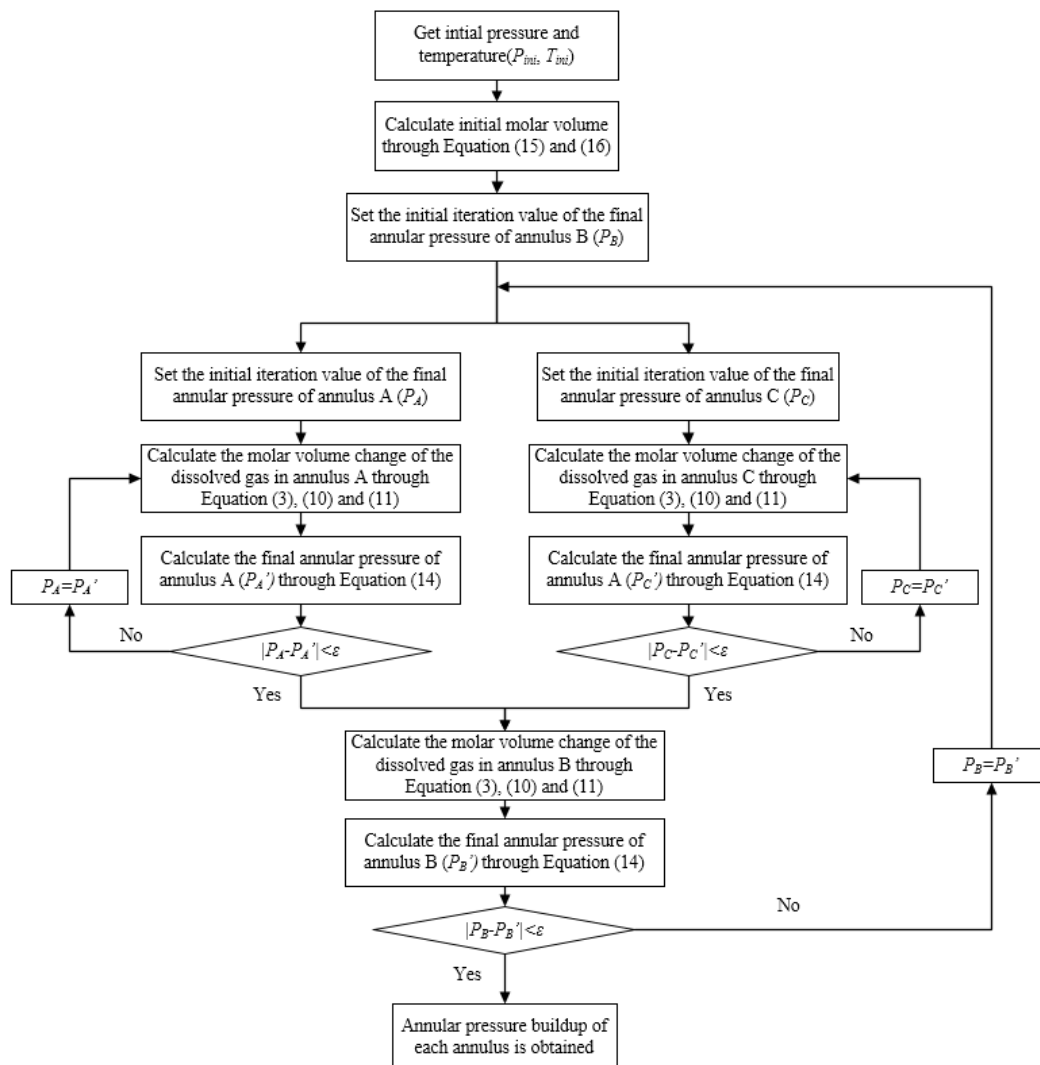


Figure 10. The calculation process of the dissolved gas model.

The dissolved gas model was used to calculate and analyze the APB, and the results were compared to that obtained with the full-liquid model. The calculation and comparison results are shown in Figure 11.

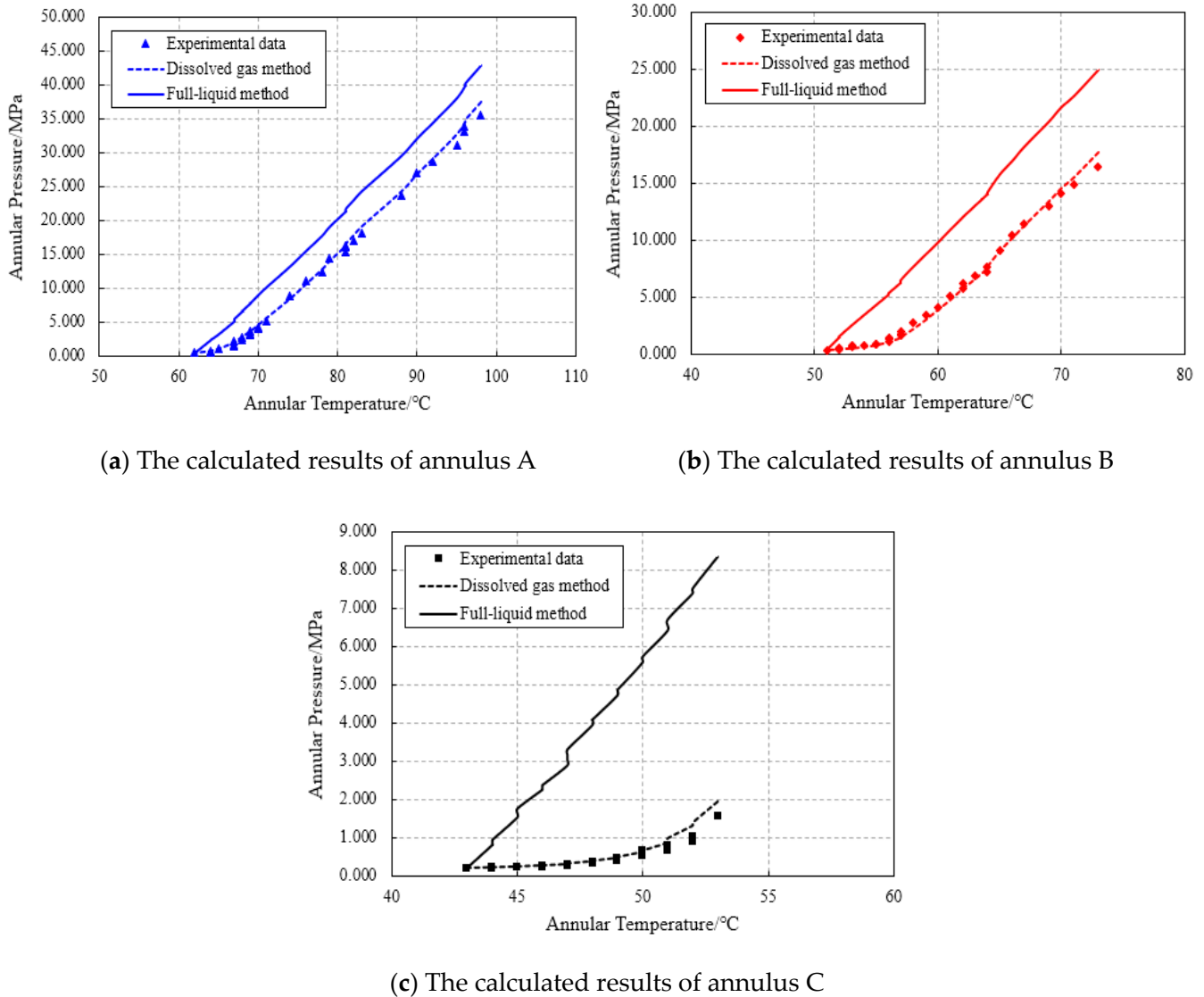


Figure 11. Comparison of the dissolved gas model simulations with experimental data and the full-liquid model results.

The error analysis of the calculated results is shown in Table 6.

Table 6. The error analysis of calculated results of the dissolved gas model.

Annulus	RMSE (MPa)	Final Prediction Error (MPa)
A	0.699	1.913
B	0.388	1.313
C	0.135	0.372

RMSE: root mean square error.

As is shown in Figure 11 and Table 6, compared with the full-liquid model, the consideration of dissolved gas can greatly improve the prediction accuracy of the APB. It is especially important for annuli B and C, which are typically harder to intervene and where a higher risk resides. For annulus B, the RMSE of the pressure prediction decreases from 5.291 MPa to 0.388 MPa, and the final prediction error decreases from 8.524 MPa to

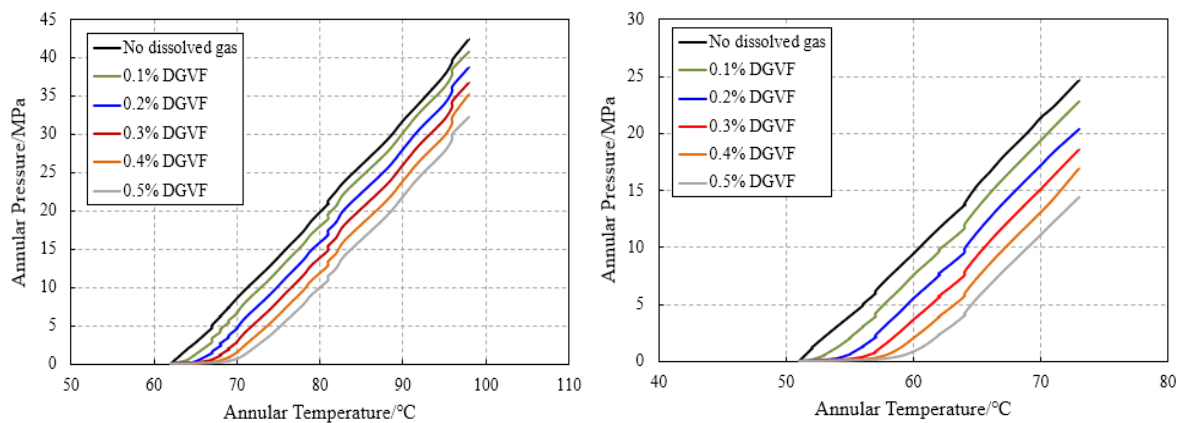
1.313 MPa, which makes the relative decrease of the final prediction error reach 84.596%. The RMSE of the pressure prediction of annulus C decreases from 3.683 MPa to 0.135 MPa and the final prediction error decreases from 6.786 MPa to 0.372 MPa, which makes the relative decrease of the final prediction error reach 94.518%.

One can therefore conclude that the influence of dissolved gas (whose volume fraction is <2% in most cases) in the modeling of an annulus full of liquid cannot be ignored. The small error in the early prediction can lead to larger error of the final annular pressure prediction. It is especially serious in high-temperature and high-pressure (HPHT) wells or offshore heavy oil thermal recovery wells. Using the dissolved gas model can reduce the overestimated error predicted by the full-liquid model, thus validating a wider scope of operations and reducing the economic cost of operations (and their contingencies).

4. Sensitivity Analysis

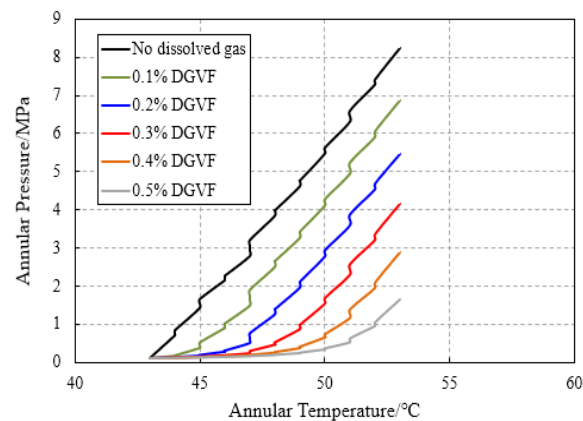
4.1. Dissolved Gas Volume Fraction

To study the influence of the dissolved gas volume fraction (DGVF) on the prediction results, a sensitivity analysis was conducted with dissolved gas volume fraction values of 0.1%, 0.2%, 0.3%, 0.4%, and 0.5%. The results are shown in Figure 12. Note that the experimental temperature data were used in the analysis and the initial pressure in each annulus was assumed to be 0.1 MPa so that the influence rule of dissolved gas content on the pressure could be better reflected. At the same time, in order to eliminate the influence of tubing pressure, it was considered that no tubing deformation is caused by internal and external pressure.



(a) The calculated results of annulus A

(b) The calculated results of annulus B



(c) The calculated results of annulus C

Figure 12. Simulation results under different dissolved gas volume fractions.

The simulation results under different dissolved gas contents were compared with those considering no dissolved gas. The comparison is provided in Table 7.

Table 7. The deviation between the results under different dissolved gas volume fraction and no dissolved gas.

		Annulus A	Annulus B	Annulus C
0.1% DGVF	RMSE (MPa)	1.732	1.858	1.200
	Final prediction error (MPa)	1.759	1.920	1.359
0.2% DGVF	RMSE (MPa)	3.599	3.592	2.155
	Final prediction error (MPa)	3.693	4.273	2.761
0.3% DGVF	RMSE (MPa)	5.312	5.064	2.870
	Final prediction error (MPa)	5.770	6.049	4.077
0.4% DGVF	RMSE (MPa)	6.811	6.305	3.371
	Final prediction error (MPa)	7.211	7.753	5.346
0.5% DGVF	RMSE (MPa)	8.219	7.439	3.691
	Final prediction error (MPa)	10.214	10.318	6.600

RMSE: root mean square error.

According to the simulations, the pressure value from which the pressure–temperature curve slope becomes stable is associated with the dissolved gas volume fraction in each annulus. The smaller the dissolved gas volume fraction is, the closer the calculated results are to the full-liquid model. When dissolved gas volume fraction is less than 0.1%, the prediction RMSE and final prediction error are both less than 2 MPa, which is acceptable for practical applications. The two curves are close to each other, which makes the small bend nearly unnoticeable. As a consequence, for all practical purposes, the full-liquid model could be used for convenience when the dissolved gas volume fraction is less than 0.1%.

4.2. Casing Deformation

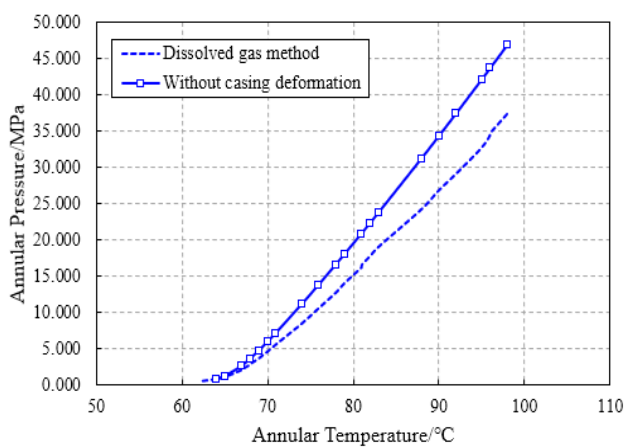
A simplified model ignoring the casing deformation is sometimes used to predict the APB [31,34]. In this work, the analysis was conducted when considering the casing as a rigid body, and the results were compared with those obtained using the dissolved gas model. Comparison of the results is shown in Figure 13.

The error analysis of the simulation results is shown in Table 8.

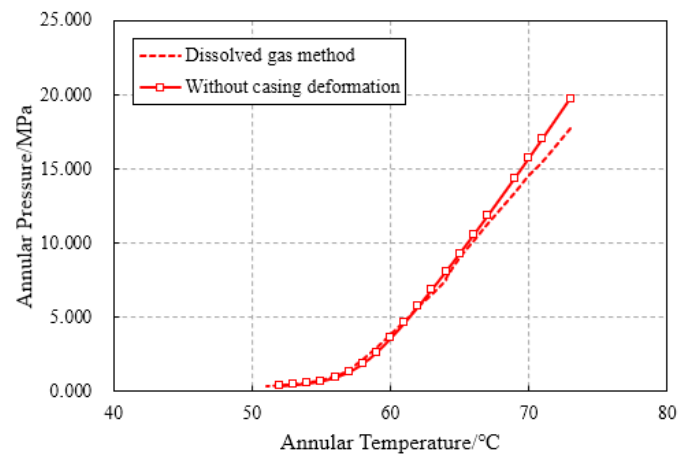
Table 8. The error analysis of calculated results without consideration of casing deformation.

Annulus	RMSE (MPa)	Final Prediction Error (MPa)
A	5.299	11.394
B	0.915	3.365
C	0.169	−0.714

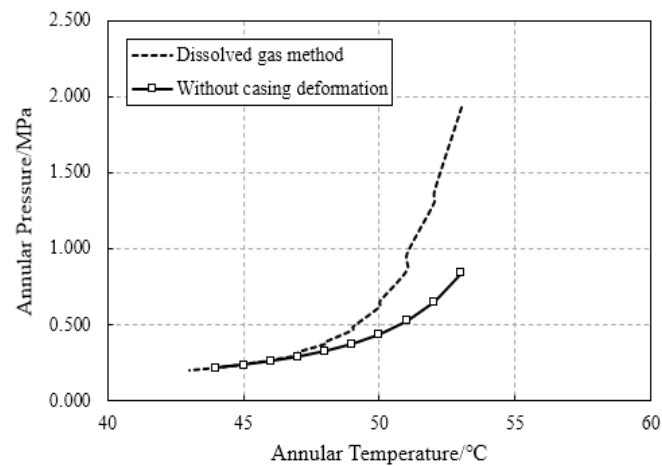
RMSE: root mean square error.



(a) The calculated results of annulus A



(b) The calculated results of annulus B



(c) The calculated results of annulus C

Figure 13. Simulation results without consideration of casing deformation.

Figure 13 shows the simulation results without taking into consideration casing deformation and its deviation from that obtained using the dissolved gas model, which considers the elasticity of casings. The volume change of annulus A is mainly caused by the outward deformation of the production casing. Therefore, treating the casing as a rigid body will lead to larger prediction results and the final prediction error reaches 11.394 MPa. However, the situation of annulus C is quite reversed. The volume change of annulus C is mainly caused by the deformation of the intermediate casing. The influence of the deformation of the surface casing is very small. Treating the casing as a rigid body will lead to lower prediction results of annulus C, the final prediction error reaching -0.714 MPa. For annulus B, the annular volume change is mainly caused by the deformation of both production and intermediate casings. The deformation of these two casings has a certain offset effect, which makes the prediction error of annulus B relatively small. To conclude, when the annulus pressure is estimated in a temperature environment similar to that of this experiment, not considering casing deformation will lead to the overestimation of pressure in annulus A and the underestimation of pressure in annulus C. For annulus B, the simplified estimation can be carried out in this experiment, but errors still exist. Therefore, the simplified model should be very carefully used according to the field temperature environment.

5. Conclusions

Based on the research in this paper, the following conclusions and operation suggestions are obtained as follows:

- (1) In this paper, the radial full-size physical simulation experiment of APB was carried out and an annular pressure prediction model taking into account dissolved gas was proposed. The modified full-liquid model and the dissolved gas model were compared and analyzed based on the experimental data. The accuracy of the model was verified.
- (2) With the decrease of the dissolved gas volume fraction, the prediction results of the dissolved gas model are closer to those of the full-liquid model. When the volume fraction of dissolved gas is less than 0.1%, the prediction RMSE and final prediction error of each annulus between the full-liquid model and dissolved gas model will be both less than 2 MPa, which is acceptable for practical application.
- (3) Analysis results indicate that the dissolved gas does exist in the annulus, and by including it in the model one obtains greater prediction accuracy. Ignoring the existence of the dissolved gas will result in an overestimation of the pressure buildup and unnecessary economic loss. If the prediction process needs to be simplified, it is recommended that the full-liquid model should be used only when the dissolved gas volume fraction is less than 0.1%.
- (4) The casing deformation of each annulus cannot be ignored for the sake of annular pressure prediction. Ignoring the casing deformation will lead to an overestimation of the pressure in annulus A and an underestimation of the pressure in annulus C. According to the experiment, the casing deformation around annulus B has an offset effect. The rigid casing model could be used in annulus B in an environment similar to that of the experiment. Therefore, the rigid casing model should be used carefully based on the field temperature conditions.

Author Contributions: All the authors conceived and designed the study. Formal analysis, H.W. and H.Z.; writing—original draft, H.W.; writing—review and editing, J.L. (Jun Li), A.C., J.L. (Jun Liu), T.S., and C.L. All authors have read and agreed to the published version of the manuscript.

Funding: This research was funded by the National Natural Science Foundation of China (Grant No. U1762211, Grant No. 51734010, Grant No. U19B6003), the CNPC strategic cooperation project (Grant No. ZLZX2020-01), the National Natural Science Foundation of China (Grant No. 52074018, Grant No. 71801198).

Acknowledgments: The authors gratefully acknowledge the help from the State Key Laboratory of Petroleum Resources and Engineering, and the State Key Laboratory of Shale Oil and Gas Enrichment Mechanisms and Effective Development.

Conflicts of Interest: The authors declare that there is no conflict of interests regarding the publication of this paper.

Nomenclature

ΔP	annular pressure buildup (MPa)
ΔT	annular fluid temperature increase (K)
α_{isob}	isobaric thermal expansion coefficient of annular fluid (1/K)
k_{isot}	isothermal compressibility of annular fluid (1/MPa)
V_{ann}	volume of the annulus (m ³)
ΔV_{ann}	volume change of the annulus (m ³)
V_l	initial volume of the annular fluid (m ³)
ΔV_l	inflow and outflow volume of the annular fluid (m ³)
P	annular fluid pressure (MPa)
V	annular fluid volume (m ³)

T	annular fluid temperature (K)
t	annular fluid temperature ($^{\circ}\text{C}$), $t = T - 273.15$
T_{fin}	final annular fluid temperature (K)
t_{fin}	final annular fluid temperature ($^{\circ}\text{C}$), $t_{fin} = T_{fin} - 273.15$
T_{ini}	initial annular fluid temperature (K)
t_{ini}	initial annular fluid temperature ($^{\circ}\text{C}$), $t_{ini} = T_{ini} - 273.15$
P_{fin}	final annular pressure (MPa)
P_{ini}	initial annular pressure (MPa)
V_{fin}	final annular fluid volume (m^3)
V_{ini}	initial annular fluid volume (m^3)
V_{int}	intermediate annular fluid volume (m^3)
u_t	casing deformation caused by thermal expansion (m)
u_p	casing deformation caused by internal and external pressure (m)
μ	Poisson's ratio
α_c	linear expansion coefficient of the casing (1/K)
r	radius of calculation position (m)
r_i	inner radius of the casing (m)
r_o	external radius of the casing (m)
E	elastic modulus (MPa)
P_o	external pressure of the casing (MPa)
P_i	inner pressure of the casing (MPa)
C	nitrogen solubility ($\mu\text{mol}/\text{kg}$)
A_0	solubility coefficient, $A_0 = 6.42931$
A_1	solubility coefficient, $A_1 = 2.92704$
A_2	solubility coefficient, $A_2 = 4.32531$
A_3	solubility coefficient, $A_0 = 4.69149$
R	Gas constant ($\text{J}\cdot\text{mol}^{-1}\cdot\text{K}^{-1}$), $R = 8.314 \text{ J}\cdot\text{mol}^{-1}\cdot\text{K}^{-1}$
\tilde{v}	gas molar volume (m^3)
P_r	reduced pressure, $P_r = P/P_c$
T_r	reduced temperature, $T_r = T/T_c$
P_c	critical pressure (MPa), $P_c = 3.394 \text{ MPa}$ for nitrogen
T_c	critical temperature (K), $T_c = 126.15 \text{ K}$ for nitrogen
a	attraction parameter of EOS, $a = [1 + m(1 - T_r^{0.5})]^2$
a_c	attraction parameter of EOS, $a_c = 0.457235R^2T_c^2/P_c$
b	co-volume parameter of EOS, $b = 0.077796RT_c/P_c$
m	formula parameters, $m = 0.374640 + 1.54226\omega - 0.26992\omega^2$
ω	Pitzer's acentric factor, $\omega = 0.045$ for nitrogen
Z	compression factor

References

1. Amaechi, C.V.; Gillett, N.; Odijie, A.C.; Hou, X.; Ye, J. Composite risers for deep waters using a numerical modelling approach. *Compos. Struct.* **2019**, *210*, 486–499. [[CrossRef](#)]
2. Amaechi, C.V.; Wang, F.; Hou, X.; Ye, J. Strength of submarine hoses in Chinese-lantern configuration from hydrodynamic loads on CALM buoy. *Ocean. Eng.* **2019**, *171*, 429–442. [[CrossRef](#)]
3. Amaechi, C.V.; Ye, J.; Hou, X.; Wang, F. Sensitivity Studies on Offshore Submarine Hoses on CALM Buoy with Comparisons for Chinese-Lantern and Lazy-S Configuration. In Proceedings of the 38th International Conference on Ocean, Offshore and Arctic Engineering, Glasgow, Scotland, UK, 9–14 June 2019. OMAE2019-96755.
4. Amaechi, C.V.; Ye, J. A numerical modeling approach of composite risers for deep waters. In Proceedings of the 20th International Conference on Composite Structures (ICCS20), Paris, France, 4–7 September 2017.
5. Sukumar, S.; Weijermars, R.; Alves, I.; Noynaert, S. Analysis of Pressure Communication between the Austin Chalk and Eagle Ford Reservoirs during a Zipper Fracturing Operation. *Energies* **2019**, *12*, 1469. [[CrossRef](#)]
6. Dong, G.; Chen, P. A review of the evaluation methods and control technologies for trapped annular pressure in deepwater oil and gas wells. *J. Nat. Gas. Sci. Eng.* **2017**, *37*, 85–105. [[CrossRef](#)]
7. Oudeman, P.; Kerem, M. Transient behavior of annular pressure build-up in HP/HT wells. *SPE Drill. Complet.* **2006**, *21*, 234–241. [[CrossRef](#)]
8. Yang, J.; Tang, H.X.; Liu, Z.L.; Yang, L.P.; Huang, X.L.; Yan, D.; Tian, R.R. Prediction model of casing annulus pressure for deepwater well drilling and completion operation. *Pet. Explor. Dev.* **2013**, *40*, 661–664. [[CrossRef](#)]

9. Pattillo, P.D.; Cocalas, B.W.; Morey, S.C. Analysis of an annular pressure buildup failure during drill ahead. In Proceedings of the SPE Annual Technical Conference and Exhibition, Houston, TX, USA, 26–29 September 2004. SPE-89775-MS. [[CrossRef](#)]
10. Sathuvali, U.B.; Pilko, R.M.; Gonzalez, R.A.; Pai, R.M.; Sachdeva, P.; Suryanarayana, P.V. Design and performance of annular pressure build-up APB mitigation techniques. In Proceedings of the IADC/SPE Drilling Conference and Exhibition, Fort Worth, TX, USA, 1–3 March 2016. SPE-178886-MS.
11. Hasan, A.R.; Izgec, B.; Kabir, C.S. Sustaining production by managing annular pressure buildup. *SPE Drill. Complet.* **2010**, *25*, 195–203. [[CrossRef](#)]
12. Bellarby, J.; Kofoed, S.S.; Marketz, F. Annular pressure build-up analysis and methodology with examples from multifrac horizontal wells and HPHT reservoirs. In Proceedings of the SPE/IADC Drilling Conference, Amsterdam, The Netherlands, 5–7 March 2013. SPE-163557-MS. [[CrossRef](#)]
13. Foolad, Y.; Bizhani, M.; Frigaard, I.A. A comparative study of laminar-turbulent displacement in an eccentric annulus under imposed flow rate and imposed pressure drop conditions. *Energies* **2021**, *14*, 1654. [[CrossRef](#)]
14. Foroushan, H.K.; Lund, B.; Ytrehus, J.D.; Saasen, A. Cement Placement: An Overview of Fluid Displacement Techniques and Modelling. *Energies* **2021**, *14*, 573. [[CrossRef](#)]
15. Tao, C.; Rosenbaum, E.; Kutchko, B.G.; Massoudi, M. A Brief Review of Gas Migration in Oilwell Cement Slurries. *Energies* **2021**, *14*, 2369. [[CrossRef](#)]
16. Tao, C.; Kutchko, B.G.; Rosenbaum, E.; Massoudi, M. A review of rheological modeling of cement slurry in oil well applications. *Energies* **2020**, *13*, 570. [[CrossRef](#)]
17. Hasan, A.R.; Kabir, C.S. Wellbore heat-transfer modeling and applications. *J. Nat. Gas. Sci. Eng.* **2012**, *86–87*, 127–136. [[CrossRef](#)]
18. Oudemans, P.; Bacarezza, L.J. Field trial results of annular pressure behavior in a HP/HT well. *SPE Drill. Complet.* **1995**, *10*, 84–88. [[CrossRef](#)]
19. Ferreira, M.V.D.; Santos, A.R.; Vanzan, V. Thermally insulated tubing application to prevent annular pressure buildup in Brazil Offshore fields. In Proceedings of the SPE Deepwater Drilling and Completions Conference, Galveston, TX, USA, 20–21 June 2012. SPE-151044-MS. [[CrossRef](#)]
20. Sun, T.F.; Zhang, X.Q.; Liu, S.J.; Cao, Y.F.; Xie, R.J. Annular Pressure Buildup Calculation When Annulus Contains Gas. *Chem. Tech. Fuels Oils* **2018**, *54*, 484–492. [[CrossRef](#)]
21. Azzola, J.H.; Tselepidakis, D.P.; Pattillo, P.D.; Richey, J.F.; Tinker, S.J.; Miller, R.A.; Segreto, S.J. Application of vacuum insulated tubing to mitigate annular pressure buildup. In Proceedings of the SPE Annual Technical Conference and Exhibition, Houston, TX, USA, 26–29 September 2004. SPE-90232-MS. [[CrossRef](#)]
22. Guan, Z.C.; Zhang, B.; Wang, Q.; Liu, Y.W.; Xu, Y.Q.; Zhang, Q. Design of thermal-insulated pipes applied in deepwater well to mitigate annular pressure build-up. *Appl. Therm. Eng.* **2016**, *98*, 129–136. [[CrossRef](#)]
23. Zhang, B.; Guan, Z.C.; Hasan, A.R.; Lu, N.; Wang, Q.; Xu, Y.Q.; Zhang, Q.; Liu, Y.W. Development and design of new casing to mitigate trapped annular pressure caused by thermal expansion in oil and gas wells. *Appl. Therm. Eng.* **2017**, *118*, 292–298. [[CrossRef](#)]
24. Liu, Z.C.; Samuel, R.; Gonzales, A.; Kang, Y.F. Modeling and simulation of annular pressure buildup (APB) mitigation using rupture disk. In Proceedings of the SPE Deepwater Drilling and Completions Conference, Galveston, TX, USA, 14–15 September 2016. SPE-180308-MS. [[CrossRef](#)]
25. Bradford, D.W.; Fritchie, D.G.; Gibson, D.H.; Gosch, S.W.; Pattillo, P.D.; Sharp, J.W.; Taylor, C.E. Marlin failure analysis and redesign; part 1, description of failure. In Proceedings of the IADC/SPE Drilling Conference, Dallas, TX, USA, 26–28 February 2002. SPE-74528-MS. [[CrossRef](#)]
26. Ellis, R.C.; Fritchie, D.G.; Gibson, D.H.; Gosch, S.W.; Pattillo, P.D. Marlin failure analysis and redesign; part 2, redesign. In Proceedings of the IADC/SPE Drilling Conference, Dallas, TX, USA, 26–28 February 2002. SPE-74529-MS. [[CrossRef](#)]
27. Wang, H.; Zhang, H.; Li, J.; Zeng, Y.J.; Ding, S.D.; Tao, Q. Optimization of the Annulus Nitrogen Injection Volume in Offshore Wells With Annular Pressure Buildup. In Proceedings of the SPE Kingdom of Saudi Arabia Annual Technical Symposium and Exhibition, Dammam, Saudi Arabia, 23–26 April 2018. SPE-192443-MS. [[CrossRef](#)]
28. Loder, T.; Evans, J.H.; Griffith, J.E. Prediction of and effective preventative solution for annular fluid pressure buildup on subsea completed wells—case study. In Proceedings of the SPE Annual Technical Conference and Exhibition, Denver, CO, USA, 5–8 October 2003. SPE-84270-MS. [[CrossRef](#)]
29. Kan, C.B.; Yang, J.; Yu, X.C.; Wang, Y.B. A novel mitigation on deepwater annular pressure buildup: Unidirectional control strategy. *J. Petrol. Sci. Eng.* **2018**, *162*, 577–587. [[CrossRef](#)]
30. Yin, F.; Gao, D.L. Improved calculation of multiple annuli pressure buildup in subsea HPHT wells. In Proceedings of the IADC/SPE Asia Pacific Drilling Technology Conference, Bangkok, Thailand, 25–27 August 2014. SPE-170553-MS. [[CrossRef](#)]
31. Liu, J.G.; Fan, H.H.; Peng, Q.; Deng, S.; Kang, B.; Ren, W.Y. Research on the prediction model of annular pressure buildup in subsea wells. *J. Nat. Gas. Sci. Eng.* **2015**, *27*, 1677–1683. [[CrossRef](#)]
32. Zhang, B.; Guan, Z.; Zhang, Q. Prediction and analysis on annular pressure of deepwater well in the production stage. *Acta Petrol. Sin.* **2015**, *32*, 1012–1017.
33. Gao, D.L.; Feng, Q.; Zheng, H.K. On a method of prediction of the annular pressure buildup in deepwater wells for oil & gas. *CMES-Comp. Model. Eng. Sci.* **2012**, *89*, 1–15.

34. Wang, L.S.; Gao, B.K.; Gao, L.; Hu, T.X. Prediction of annular pressure caused by thermal expansion by considering the variability of fluid properties. *Appl. Therm. Eng.* **2018**, *141*, 234–244. [[CrossRef](#)]
35. Wang, L.S.; Gao, B.K.; Gao, L.; Hu, T.X. Design and application of foamed spacer to mitigate annular pressure induced by fluid thermal expansion. *Appl. Therm. Eng.* **2020**, *165*, 114524. [[CrossRef](#)]
36. Vargo, R.F., Jr.; Payne, M.; Faul, R.; LeBlanc, J.; Griffith, J.E. Practical and successful prevention of annular pressure buildup on the Marlin project. In Proceedings of the SPE Annual Technical Conference and Exhibition, San Antonio, TX, USA, September 29–October 2 2002. SPE-77473-MS. [[CrossRef](#)]
37. Zhang, B.; Guan, Z.C.; Sheng, Y.N.; Wang, Q.; Xu, C.B. Impact of wellbore fluid properties on trapped annular pressure in deepwater wells. *Pet. Explor. Dev.* **2016**, *43*, 869–875. [[CrossRef](#)]
38. Kulkarni, S.D.; Vyas, A.; Gupta, H. Evaluating precision of fluid/casing design for annular pressure build-up APB application using machine-learning tools. In Proceedings of the SPE Annual Technical Conference and Exhibition, Calgary, AB, Canada, 30 September–2 October 2019. SPE-196179-MS. [[CrossRef](#)]
39. Santos, H.L.; Rocha, J.S.; Ferreira, M.V.; Lima, V.; Souza, C.O.; Borges, A.; Silva, E.C. APB mitigation techniques and design procedure. In Proceedings of the OTC Brasil, Rio de Janeiro, Brazil, 27–29 October 2015. OTC-26294-MS. [[CrossRef](#)]
40. Zhou, B.; Yang, J.; Liu, Z.L.; Luo, J.F.; Huang, X.L.; Zhou, R.X.; Song, Y. Mechanism of pressure management by injecting nitrogen in casing annulus of deepwater wells. *Pet. Explor. Dev.* **2015**, *42*, 422–426. [[CrossRef](#)]
41. Williamson, R.; Sanders, W.; Jakabosky, T.; Serio, M.; Griffith, J.E. Control of contained-annulus fluid pressure buildup. In Proceedings of the SPE/IADC Drilling Conference, Amsterdam, Netherlands, 19–21 February 2003. SPE-79875-MS. [[CrossRef](#)]
42. Yang, G.T. *Introduction to Elasticity and Plasticity*; Tsinghua University Press: Beijing, China, 2004.
43. Colt, J. *Computation of Dissolved Gas Concentration in Water as Functions of Temperature, Salinity and Pressure*; Elsevier: Waltham, MA, USA, 2012.
44. Danesh, A. *PVT and Phase Behaviour of Petroleum Reservoir Fluids*; Elsevier Science B.V.: Amsterdam, The Netherlands, 1998.